Inorganic Chemistry
Article

Inorg. Chem. **2010**, *49*, 9151–9161 **9151**
DOI: 10.1021/ic1002594

Photophysical Properties of the Series *fac*- and *mer*-(1-Phenylisoquinolinato-N^C$^{2'}$)$_x$(2-phenylpyridinato-N^C$^{2'}$)$_{3-x}$Iridium(III) (x = 1−3)†

Joseph C. Deaton,*,‖,‡ Ralph H. Young,⊥,‡ Jerome R. Lenhard,‡ Manju Rajeswaran,‡ and Shouquan Huo*,§

‡*Eastman Kodak Company, Rochester, New York 14650, and* §*Department of Chemistry, East Carolina University, Greeneville, North Carolina 27858.* ‖*Current address: Department of Chemistry, Bowling Green State University, Bowling Green, Ohio 43403.* ⊥*Current address: Department of Chemistry, University of Rochester, Rochester, New York 14627.*

Received February 8, 2010

The photophysical properties of tris-cyclometalated iridium(III) complexes have been probed by chemical and geometric variation through the series *fac*- and *mer*-Ir(piq)$_x$(ppy)$_{3-x}$ (x = 1−3; piq = 1-phenylisoquinolinato-N^C$^{2'}$, ppy = 2-phenylpyridinato-N^C$^{2'}$). The phosphorescent decays were recorded in solution at 295 K and in polymer films from 2 to 295 K. In the heteroleptic complexes, emission occurs based solely on the piq ligand(s), at least by the nanosecond time scale, as its excited states are the lowest energy. Because *fac*-Ir(piq)$_3$ and *fac*-Ir(ppy)$_3$ possess practically the same oxidation potential, comparison of photophysical properties through the series *fac*-Ir(piq)$_x$(ppy)$_{3-x}$ (x = 1−3) revealed the effects of having one, two, or three emissive piq ligands with no confounding effects from differences in electron withdrawing or donating properties between the spectator ppy ligands and the piq ligands. Effects of placement of piq ligands in different coordination geometries were elucidated by comparisons to the *mer* series.

Introduction

Since the pioneering work on organic light-emitting diodes (OLEDs) comprising amorphous thin films by scientists at Eastman Kodak Company,[1,2] the technology has been vigorously pursued for application in flat-panel displays and energy-efficient lighting. C^N-cyclometalated complexes of iridium(III), such as the green emissive *fac*-Ir(ppy)$_3$ (ppy = 2-phenylpyridinato-N^C$^{2'}$)[3,4] and the red *fac*-Ir(piq)$_3$ (piq = 1-phenylisoquinolinato-N^C$^{2'}$),[5] are now well known for applications as phosphorescent emitters in OLEDs.[6−10] Because the phosphorescent emitters are capable of harvesting both the singlet and the triplet excitons that are formed by charge recombination in the device, they offer the potential to attain 100% internal quantum efficiency (IQE) of photons produced per electron passed through the device, while fluorescent emitters are limited to 25% IQE because they are capable of harvesting only the singlet excitons as useful light.[11]

Devices doped with Ir complexes have been reported to have external quantum efficiencies (EQE, photons per electron) in the range of 20−29% with no optical outcoupling enhancements.[12−16] A model based on classical ray optics for outcoupling predicts a maximum possible outcoupling of

† Work carried out at Eastman Kodak Company, Rochester, New York 14650, was done prior to December 2009.

*To whom correspondence should be addressed. E-mail: jdeaton@bgsu.edu (J.C.D.); huos@ecu.edu (S.H.).

(1) Tang, C. W.; Van Slyke, S. A. *Appl. Phys. Lett*. **1987**, *51*, 913–915.
(2) Tang, C. W.; Van Slyke, S. A.; Chen, C. H. *J. Appl. Phys*. **1989**, *65*, 3610–3616.
(3) King, K. A.; Spellane, P. J.; Watts, R. J. *J. Am. Chem. Soc*. **1985**, *107*, 1431.
(4) Dedeian, K.; Djurovich, P. I.; Garces, F. O.; Carlson, G.; Watts, R. J. *Inorg. Chem*. **1991**, *30*, 1687.
(5) Tsuboyama, A.; Iwawaki, H.; Furugori, M.; Mukaide, T.; Kamatani, J.; Igawa, S.; Moriyama, T.; Miura, S.; Takiguchi, T.; Okada, S.; Hoshino, M.; Ueno, K. *J. Am. Chem. Soc*. **2003**, *125*, 12971–12979.
(6) Baldo, M. A.; Lamansky, S.; Burrows, P. E.; Thompson, M. E.; Forrest, S. R. *Appl. Phys. Lett*. **1999**, *75*, 4–6.
(7) Lamansky, S.; Djurovich, P.; Murphy, D.; Abdel-Razzaq, F.; Lee, H. E.; Adachi, C.; Burrows, P. E.; Forrest, S. R.; Thompson, M. E. *J. Am. Chem. Soc*. **2001**, *123*, 4304–4312.
(8) Lamansky, S.; Djurovich, P.; Murphy, D.; Abdel-Razzaq, F.; Kwong, R.; Tsyba, I.; Bortz, M.; Mui, B.; Bau, R.; Thompson, M. E. *Inorg. Chem*. **2001**, *40*, 1704–1711.
(9) Hack, M.; Weaver, M. S.; Adamovich, V.; Kwong, R. C.; Lu, M. H.; Brown, J. J. *Proc. SPIE* **2005**, *5961*, 596102−1–9.
(10) Djurovich, P. I.; Thompson, M. E. In *Highly Efficient OLEDs with Phosphorescent Materials*; Yersin, H., Ed.; Wiley-VCH Verlag GmbH & Co., KgaA: Weinheim, Germany, 2008.
(11) Baldo, M. A.; O'Brien, D. F.; You, Y.; Shoustikov, A.; Sibley, S.; Thompson, M. E.; Forrest, S. R. *Nature* **1998**, *395*, 151.
(12) Adachi, C.; Baldo, M. A.; Thompson, M. E.; Forrest, S. R. *J. Appl. Phys*. **2001**, *90*, 5048–5051.
(13) Kondakova, M. E.; Pawlik, T. D.; Young, R. H.; Giesen, D. J.; Kondakov, D. Y.; Brown, C. T.; Deaton, J. C.; Lenhard, J. R.; Klubek, K. P. *J. Appl. Phys*. **2008**, *104*, 094501–1−17.
(14) Chopra, N.; Lee, J.; Zheng, Y.; Eom, S.-H.; Xue, J.; So, F. *Appl. Phys. Lett*. **2008**, *93*, 143307–1−3.
(15) Tanaka, D.; Agata, Y.; Sasabe, S.; Li, Y.-J.; Su, S.-J.; Takeda, T.; Kido, J. *Jpn. J. Appl. Phys*. **2007**, *46*, L10–L12.
(16) Tanaka, D.; Agata, Y.; Takeda, T.; Watanabe, S.; Kido, J. *Jpn. J. Appl. Phys*. **2007**, *46*, L117–L119.

Published on Web 09/14/2010

22% from these simple bottom-emitting devices supported on glass having an index of refraction of 1.5.[17] Reports of EQE above that limit suggest that the accuracy of either the optical model[18] or the measurement needs refinement, but there seems to be a general consensus that these devices must be operating at close to 100% IQE in order to give such a high EQE.

In accord with the high quantum yield of the cyclometalated Ir complexes and their important applications, there have been detailed studies of their photophysical properties,[19−28] including studies of heteroleptic tris-C^N-cyclometalated complexes.[29,30] There have even been studies of *fac*-Ir(piq)$_x$(ppy)$_{3-x}$ (x = 1−3), including absorption and emission in solution and performance in OLEDs[31,32]

We considered the title set of complexes to be of interest for a detailed study because the oxidation potentials of the parent homoleptic complexes are nearly identical. Therefore, we propose that the presence of the ppy ligand(s) in the heteroleptic complexes should not alter the degree of metal character in the orbitals involved in the emission based on the piq ligand(s) because the electron donor properties of the two ligands are evidently the same. We also assume that on the time scale of our experiments (> ns), the emission originates from the piq ligand(s) because these provide lower energy excited states than those of the ppy ligand(s). As a consequence, the series *fac*-Ir(piq)$_x$(ppy)$_{3-x}$ (x = 1−3) should provide experimental comparison of the effects upon photophysical properties of having one, two, or three emissive piq ligands without being confounded by effects from differences in electron withdrawing or donating properties between the spectator ppy ligand and the piq ligands. One question that might be addressed through the *fac* series is whether the emissive state in *fac*-Ir(piq)$_3$ is localized on individual ligands or delocalized over all three symmetry-related ligands. According to models proposed for the isoelectronic Ru(bpy)$_3^{2+}$, excited states will be delocalized or localized depending upon the degree that ligands are coupled through shared metal orbitals[33,34] compared to the degree that inhomogeneity in a particular environment would stabilize the excited state on one particular ligand in the lowest energy environment.[35,36] It has been shown that the thermalized excited state of Ru(bpy)$_3^{2+}$ in solution becomes localized on an individual ligand as the solvent molecules reorient to stabilize the change in molecular dipole moment.[37] In contrast, a delocalized description of the excited state for Ru(bpy)$_3^{2+}$ in low temperature glasses has been the conclusion of other studies.[33,38,39] However, there has been debate in the literature on whether the excited state of Ru(bpy)$_3^{2+}$ in doped single crystals is delocalized[34,40,41] or localized.[42,43] Comparatively little attention has been paid to the question of localization or delocalization in the C^N-cyclometalated complexes of Ir(III).

Comparison to the series *mer*-Ir(piq)$_x$(ppy)$_{3-x}$ (x = 1−3) should reveal effects of placing emissive ligands in different coordination geometries. In the previous communication,[44] a highly selective synthesis was reported for each member of the series *mer*-Ir(piq)$_x$(ppy)$_{3-x}$ (x = 0−3), wherein the unique ligand in the heteroleptic complexes occupies a coordination site that is trans to the two Ir−C bonds of the other two ligands. We reported a significant blue shift of the room temperature emission when the piq ligand was in this unique coordination site in *mer*-Ir(piq)(ppy)$_2$. In the present paper, we report the preparation and isolation of *fac*-Ir(piq)(ppy)$_2$ and of *fac*-Ir(piq)$_2$(ppy), and the electrochemical potentials of both series *fac*- and *mer*-Ir(piq)$_x$(ppy)$_{3-x}$ (x = 0−3) (Chart 1). We report emission spectra and phosphorescent decay rates of both series for x = 1−3 in amorphous poly(methyl methacrylate) (PMMA) host from 295 K down to 2 K, and evaluation of the excited state zero field splittings by fits to the temperature dependence of the decay rates. We also report the electroluminescence of the *fac* series in vapor-deposited OLEDs.

Experimental Section

Materials, Synthesis, and Characterization. The syntheses of the complexes *mer*-Ir(piq)$_x$(ppy)$_{3-x}$ (x = 1−3) were reported previously.[44] The ligand 1-phenylisoquinoline[5] and the complex *fac*-Ir(piq)$_3$[45] were synthesized by the cited published procedures (Anal. calcd. for *fac*-Ir(piq)$_3$, $C_{45}H_{30}IrN_3$: C, 67.14; H, 3.6; N, 5.22, found: C, 66.89; H, 3.60; N, 5.27). Solvents and the ligand 2-phenyl pyridine were purchased from Aldrich Chemical Co. and were used as received. All reactions were carried out under nitrogen atmosphere. HPLC analysis was performed on BDS Hypersil C-18 column (100 × 3 mm) with an Agilent 1100 Series HPLC equipped with an Agilent 1100 binary pump, an

(17) Greenham, N. C.; Friend, R. H.; Bradley, D. D. C. *Adv. Mater.* **1994**, *6*, 491–494.
(18) Nowy, S.; Krummacher, B. C.; Frischeisen, J.; Reinke, N. A.; Brütting, W. *J. Appl. Phys.* **2008**, *104*, 12109-1–9.
(19) Colombo, M. C.; Brunold, T. C.; Riedener, T.; Güdel, H. U.; Förtsch, M.; Bürgi, H.-B. *Inorg. Chem.* **1994**, *33*, 545.
(20) Finkenzeller, W. J.; Yersin, H. *Chem. Phys. Lett.* **2003**, *377*, 299–305.
(21) Holzer, W.; Penzkofer, A.; Tsuboi, T. *Chem. Phys.* **2005**, *308*, 93–102.
(22) Breu, J.; Stössel, P.; Schrader, S.; Starukhin, A.; Finkenzeller, W. J.; Yersin, H. *Chem. Mater.* **2005**, *17*, 1745–1752.
(23) Marchetti, A. P.; Deaton, J. C.; Young, R. H. *J. Phys. Chem. A* **2006**, *110*, 9828–9838.
(24) Finkenzeller, W. J.; Thompson, M. E.; Yersin, H. *Chem. Phys. Lett.* **2007**, *444*, 273.
(25) Finkenzeller, W. J.; Hofbeck, T.; Thompson, M. E.; Yersin, H. *Inorg. Chem.* **2007**, *46*, 5076.
(26) Bauer, R.; Finkenzeller, W. J.; Bogner, U.; Thompson, M. E.; Yersin, H. *Org. Elect.* **2008**, *9*, 641.
(27) Rausch, A. F.; Thompson, M. E.; Yersin, H. *J. Phys. Chem. A.* **2009**, *113*, 5927–5932.
(28) Rausch, A. F.; Thompson, M. E.; Yersin, H. *Inorg. Chem.* **2009**, *48*, 1928–1937.
(29) Dedeian, K.; Shi, J.; Shepherd, N.; Forsythe, E.; Morton, D. C. *Inorg. Chem.* **2005**, *44*, 4445–4447.
(30) Karatsu, T.; Ito, E.; Yagai, S.; Kitamura, A. *Chem, Phys. Lett.* **2006**, *424*, 353–357.
(31) Rho, H. R.; Park, G. Y.; Ha, Y.; Kim, Y. S. *Jpn. J. Appl. Phys.* **2006**, *45*, 568–573.
(32) Lee, J. Y. *Appl. Phys. Lett.* **2006**, *89*, 223517–1−3.
(33) Crosby, G. A.; Elfring, W. H., Jr. *J. Phys. Chem.* **1976**, *80*, 2206–2211.
(34) Yersin, H.; Humbs, W.; Strasser, J. *Coord. Chem. Rev.* **1997**, *159*, 325–358.
(35) Kober, E. M.; Meyer, T. J. *Inorg. Chem.* **1984**, *23*, 3877–3886.
(36) Riesen, H.; Wallace, L.; Krausz, E. *J. Phys. Chem.* **1996**, *100*, 17138–17144.
(37) Yeh, A. T.; Shank, C. V.; McCusker, J. K. *Science* **2000**, *289*, 935–938.
(38) DeArmond, M. K.; Carlin, C. M.; Huang, W. L. *Inorg. Chem.* **1980**, *19*, 62–67.
(39) Ferguson, J.; Krausz, E. *J. Phys. Chem.* **1987**, *91*, 3161–3167.
(40) Yersin, H.; Humbs, W.; Strasser, J. *Top. Curr. Chem.* **1997**, *191*, 153–249.
(41) Bauer, R.; Huber, P.; Wudy, J.; Schmidt, J.; Yersin, H. *J. Phys. Chem.* **1994**, *98*, 8044–8049.
(42) Riesen, H.; Krausz, E. *J. Chem. Phys.* **1993**, *99*, 7614–7618.
(43) Riesen, H.; Wallace, L.; Krausz, E. *Inorg. Chem.* **2000**, *39*, 5044–5052.
(44) Huo, S.; Deaton, J. C.; Rajeswaran, M.; Lenhart, W. C. *Inorg. Chem.* **2006**, *45*, 3155.
(45) Deaton, J. C. U.S. Patent 2006, 7,005,522 B2.

Chart 1. Facial and Meridional $Ir(piq)_x(ppy)_{3-x}$

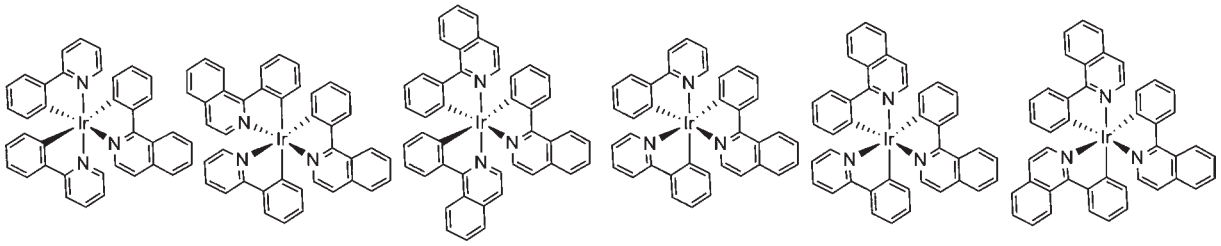

Agilent 1100 autosampler, and an Agilent 1100 diode array detector. Accurate mass measurements using mass spectrometry were performed on a Mariner time-of-flight (TOF) mass spectrometer (PerSeptive Biosystems) operating in positive ion mode. Ionization was accomplished using a TurboIon Spray (electrospray) source. The instrument was operated in full scan mode from m/z 100−1200 at a rate of 2 s per spectrum. The mass spectrometer was mass calibrated just prior to the chromatographic analysis. ^{1}H and ^{13}C NMR spectra were recorded on a Varian Inova 500 spectrometer. Chemical shifts were referenced to TMS @ 0 ppm for ^{1}H and CD_2Cl_2 @ 54.0 ppm for ^{13}C.

Preparation of *fac*-Ir(piq)$_2$(ppy), Method A. A dry flask was charged with *mer*-Ir(piq)$_2$(ppy) (400 mg, *mer*/*fac* ratio >99:1 by HPLC peak area) and anhydrous tetradecane (20 mL). The mixture was refluxed under nitrogen atmosphere for 2 h. After being cooled to room temperature, the mixture was diluted with heptane and filtered. The crude material contained 97% (by HPLC peak area) *fac*-Ir(1-piq)$_2$(ppy) and 3% *mer*-Ir(1-piq)$_2$-(ppy). The crude material was dissolved in dichloromethane and filtered through a silica gel plug and washed with dichloromethane. The filtrate was concentrated and the product *fac*-Ir-(1-piq)$_2$(ppy) was precipitated by addition of methanol, 328 mg, 82%, >97% isomeric purity. The material was sublimed at 270 °C to give deep red crystals with >99% HPLC isomeric purity. ^{1}H NMR (500 MHz, CD_2Cl_2), δ 8.98 (m, 2H), 8.22 (t, J = 8.60 Hz, 2H), 7.94 (d, J = 8.22 Hz, 1H), 7.82 (m, 1H), 7.78 (m, 1H), 7.71−7.62 (m, 6H), 7.49 (d, J = 6.15 Hz, 1H), 7.43 (m, 1H), 7.38 (d, J = 6.22 Hz, 1H), 7.27 (d, J = 6.26 Hz, 1H), 7.17 (d, J = 6.22 Hz, 1H), 7.20−6.72 (m, 3H), 6.92−6.82 (m, 4H), 6.82−6.75 (m, 2H), 6.70 (d, J = 7.81 Hz, 1H) ppm. ^{13}C NMR (125 MHz, CD_2Cl_2), δ 167.84, 167.62, 166.69, 165.14, 164.53, 161.61, 147.75, 145.75, 145.72, 144.27, 140.23, 139.82, 137.50, 137.26, 137.20, 137.07, 137.03, 136.57, 130.66, 130.64, 130.61, 130.55, 130.07, 130.00, 129.91, 128.00, 127.85, 127.45, 127.43, 126.86, 126.83, 124.31, 122.55, 120.83, 120.76, 120.32, 119.85, 119.69, 119.30 ppm. Anal. Calcd for $C_{41}H_{28}IrN_3$: C, 65.23; H, 3.74; N, 5.57; found: C, 65.07; H, 3.65; N, 5.61. MS: m/z calcd for $C_{41}H_{28}{}^{191}IrN_3$: 753.1917; found 753.1923 .

Preparation of *fac*-Ir(piq)$_2$(ppy), Method B. A mixture of *mer*-Ir (piq)$_2$(ppy) (300 mg, 0.4 mmol), dichloromethane (30 mL), acetic acid (48 mg, 0.8 mmol), and silica gel (2 g, 60−200 mesh, Aldrich) was stirred at room temperature for 24 h. The mixture was filtered through a short column packed with silica gel and washed with dichloromethane. The filtrate was concentrated and addition of methanol led to the precipitation of the product. The precipitates were collected by filtration, washed with methanol and ether, and dried in air to yield 110 mg of *fac*-Ir-(piq)$_2$(ppy), 37%, >98% HPLC isomeric purity.

Preparation of *fac*-Ir(piq)(ppy)$_2$. Tetrakis(2-phenylpyridinato-N^C$^{2'}$)(μ-dibromo)diiridium(III) (0.5 mmol), silver triflate (1 mmol), 1-phenylisoquinoline (3 mmol), and 2-ethoxyethanol (20 mL) were combined and placed under nitrogen. The mixture was refluxed for 24 h and then filtered to remove AgBr and precipitated products. The products were washed out with CH_2Cl_2 and were found to comprise a mixture of *fac*-Ir(piq)$_x$-(ppy)$_{3-x}$ (x = 0−3). The mixture was chromatographed on silica gel with CH_2Cl_2/heptane, first 1:2 (v/v), followed by 1:1 (v/v). The fractions were monitored by HPLC and those enriched in *fac*-Ir(piq)(ppy)$_2$ (87% HPLC area) were combined and evaporated to dryness. The crude material was redissolved in CH_2Cl_2 and precipitated by addition of methanol. The steps of chromatography and precipitation were repeated three times to improve the purity of the desired product to 95%, with 5% of *fac*-Ir(piq)$_2$(ppy) as the main impurity. ^{1}H NMR (500 MHz, CD_2Cl_2), δ 8.97 (m, 1H), 8.22 (d, J = 8.19 Hz, 1H), 7.94 (t, J = 7.98 Hz, 2H), 7.81 (m, 1H), 7.70−7.60 (m, 6H), 7.56 (m, 1H), 7.48 (d, J = 6.33 Hz, 1H), 7.41 (m, 1H), 7.25 (d, 6.03 Hz,1H), 7.00−6.70 (m, 10H), 6.67 (d, 7.62 Hz, 1H) ppm. ^{13}C NMR (125 MHz, CD_2Cl_2), δ 167.99, 167.08, 166.85, 164.95, 162.05, 161.35, 148.11, 147.59, 145.88, 144.48, 144.45, 140.15, 137.57, 137.49, 137.28, 137.25, 136.80, 136.78, 130.85, 130.81, 130.29, 130.21, 130.17, 128.20, 128.06, 127.65, 127.03, 124.59, 124.54, 122.73, 122.70, 120.96, 120.56, 120.41, 119.93, 119.49, 119.45 ppm. Anal. Calcd for $C_{37}H_{26}IrN_3$: C, 63.05; H, 3.72; N, 5.96; found: C, 63.47; H, 3.77; N, 5.74. HRMS: m/z calcd for $C_{37}H_{26}{}^{191}IrN_3$: 703.1761; found 703.1743.

X-ray Crystallography. A red thin plate shaped crystal of *fac*-Ir(piq)$_2$(ppy) of approximate dimensions 0.05 × 0.15 × 0.45 mm was chosen for data collection. Single crystal diffraction data were collected at 293 K using a Nonius KappaCCD diffractometer with graphite monochromated MoKα radiation (λ = 0.71073 Å) using fine-focus sealed tube. A total of 189 diffraction frames was collected using $\phi + \omega$ scans to fill the asymmetric unit with a scan range of 1.6° and a counting time of 16 s per frame. The first 10 frames were used for indexing reflections using DENZO[46] package and refined to obtain final cell parameters. Data reductions were performed using DENZO-SMN.[46] A numerical absorption correction was applied using the SORTAV[47] program. The structure was solved by using the direct methods, and refined by full-matrix least-squares on F^2 with anisotropic displacement parameters for the non-hydrogen atoms using SHELXTL.[48] Before the final least-squares cycles, hydrogen atoms were placed in idealized positions and refined as riding atoms with isotropic displacement parameters. Details of the crystallography and crystal parameters are given in Table 1. Crystallographic data for the structure reported in this paper have been deposited with the Cambridge Crystallographic Data Centre as supplementary publication no. CCDC 764332. Copies of the data can be obtained free of charge from www.ccdc.cam.ac.uk/conts/retrieving.html.

Electrochemistry. Electrochemical potentials were obtained by phase-selective second-harmonic AC voltammetry (SHACV) using the quadrature component at an applied frequency of 400 Hz (16 mV peak-to-peak signal) as described previously.[49]

(46) Otwinowski, Z.; Minor, W. *Methods in Enzymology, 276: Macromolecular Crystallography, Part A*; Carter, C. W., Jr., Sweets, R. M., Eds.; Academic Press: New York; pp 307−326.

(47) The SORTAV program is based on the method of Blessing; see Blessing, R. H. *Acta Crystallogr. A* **1995**, *51*, 33.

(48) *SHELXTL: Structure Analysis Program*, version 6.10; Bruker Analytical X-ray systems: Madison, WI, 2001.

(49) Lenhard, J. *J. Imag. Sci.* **1986**, *30*, 27.

Table 1. Crystal Data and Structure Refinement for *fac*-Ir(piq)$_2$(ppy)

empirical formula	$C_{41}H_{28}IrN_3$	
formula weight	754.86	
temperature	293(2) K	
wavelength	0.71073 Å	
crystal system	monoclinic	
space group	$P2(1)/n$	
unit cell dimensions	a = 11.2923(3) Å	α = 90°
	b = 20.9617(6) Å	β = 101.3760(10)°
	c = 12.7861(5) Å	γ = 90°
volume	2967.08(16) Å^3	
Z	4	
density (calculated)	1.690 Mg/m^3	
absorption coefficient	4.536 mm^{-1}	
F(000)	1488	
crystal size	0.05 × 0.15 × 0.45 mm^3	
theta range for data collection	3.54−27.49°	
index ranges	$-14 \le h \le 14$, $-24 \le k \le 26$, $-16 \le l \le 14$	
reflections collected	25191	
independent reflections	6646 [R(int) = 0.2197]	
completeness to theta = 27.49°	97.7%	
absorption correction	multiscan	
refinement method	full-matrix least-squares on F^2	
data/restraints/parameters	6646/0/406	
goodness-of-fit on F^2	0.832	
final R indices [$I > 2\sigma(I)$]	R_1 = 0.0532, wR_2 = 0.0893	
R indices (all data)	R_1 = 0.1624, wR_2 = 0.1178	
largest diff peak and hole	1.342 and −1.791 e Å^{-3}	

Solutions for voltammetry were prepared in CH_3CN/toluene (1:1) mixture and contained 0.1 M tetrabutylammonium tetrafluoroborate ($TBABF_4$) and were deaerated with argon prior to examination. The working electrode was a gold disk (Bioanalytical Systems, 0.02 cm^2) that was polished with 1-μm diamond paste (Buhler Metadi), rinsed with water, and dried before each experiment. All potentials were measured vs the NaCl-saturated calomel electrode (SCE) at 22 °C. Ferrocene was used as an internal standard.

Photophysical Measurements. Steady-state emission spectra were recorded as previously reported,[23] except the excitation source was the 457−458 nm line of an Ar ion laser. Luminescence decay at variable temperatures was recorded as previously reported,[23] except the excitation source was coumarin dye laser tuned to 485 nm that was pumped by a YAG laser. An integrating sphere method of measuring quantum yield of the iridium complexes in PMMA at 295 K (475 nm excitation) using a ∼1 mm thick casting prepared by slow evaporation of a solution containing PMMA and a compound at 0.015% by weight was described previously.[50] Comparison samples of rhodamine 6G in PMMA gave values of $\Phi = 0.92$. Solution quantum yields were measured in deoxygenated 2-MeTHF solution using quinine sulfate in 1 N H_2SO_4 and an excitation wavelength of 355 nm.[51]

OLED Device Fabrications and Evaluation. Vapor pressure measurements and OLED device fabrication and evaluation were performed as described previously.[50] Color is reported in 1931 CIE coordinates. Host and transport materials used in the fabrication of devices were synthesized at Eastman Kodak Company or were purchased commercially.

Results and Discussion

Synthesis. The *mer*-Ir(piq)$_x$(ppy)$_{3-x}$ were synthesized as described in the previous communication.[44] The high purity of the meridional compounds, particularly without contamination by any facial isomers, is essential to the study, since the facial isomer usually emits much more efficiently.

Photochemical isomerization of blue and green emissive meridional tris-cyclometalated iridium complexes into their corresponding facial complexes has been reported.[29,52−54] However, we did not observe any isomerization of *mer*-Ir(piq)$_3$ or *mer*-Ir(piq)$_2$(ppy) under the same photochemical conditions. We speculate that the photoisomerization could be promoted by a d−d state which is thermally accessible in the case of the green and blue emitters, but not in the red emitters.

Most methods for synthesis of *fac* complexes are carried out in high-boiling alcohol solvents and proceed through a kinetic intermediate of the *mer* complex, such as the method used here to synthesize *fac*-Ir(piq)$_3$. However, use of such methods to form heteroleptic *fac* complexes invariably results in mixtures of all four complexes Ir$L_xL'_{3-x}$ (x = 0−3).[29,52] This has been our experience, too, and seems to have been the result in an earlier report on *fac*-Ir(piq)$_2$(ppy).[31] A method has recently been reported in which *fac* isomers were formed at lower temperatures apparently without going through *mer* intermediates, but this method was not applied to heteroleptic complexes.[55] In the present study, conditions were found for the thermal isomerization of *mer*-Ir(piq)$_2$(ppy) in tetradecane to the facial isomer with relatively little ligand scrambling. It was also possible to carry out the isomerization in the neat solid state (Supporting Information).

Alternatively, we discovered that simply stirring a mixture of *mer*-Ir(piq)$_2$(ppy), acetic acid, and silica gel in dichloromethane at room temperature cleanly produced *fac*-Ir(piq)$_2$(ppy). Although the yield was low (37%), there were no ligand scrambling products. The presence

(50) Deaton, J. C.; Place, D. W.; Brown, C. T.; Rajeswaran, M.; Kondakova, M. E. *Inorg. Chim. Acta* **2008**, *361*, 1020–1035.
(51) Eaton, D. F. *Pure Appl. Chem.* **1988**, *60*, 1107.
(52) McDonald, A. R.; Lutz, M.; von Chrzanowski, L. S.; van Klink, G. P. M.; Spek, A. L.; van Koten, G. *Inorg. Chem.* **2008**, *47*, 6681–6691.
(53) Tamayo, A.; Alleyne, B. D.; Djurovich, P. I.; Lamansky, S.; Tsyba, I.; Ho, N. N.; Bau, R.; Thompson, M. E. *J. Am. Chem. Soc.* **2003**, *125*, 7377.
(54) Karatsu, T.; Nakamura, T.; Yagai, S.; Kitamura, A.; Yamaguchi, K.; Matsushima, Y.; Iwata, T.; Hori, Y.; Hagiwara, T. *Chem.. Lett.* **2003**, *32*, 886–887.
(55) McGee, K. A.; Mann, K. R. *Inorg. Chem.* **2007**, *46*, 7800–7809.

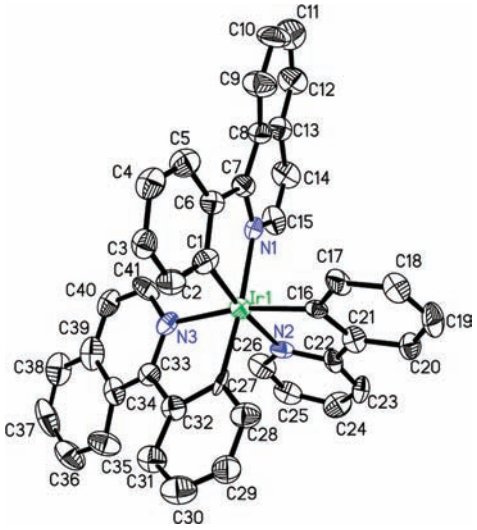

Figure 1. An ORTEP diagram showing atomic numbering scheme for *fac*-Ir(piq)$_2$(ppy). Thermal ellipsoids were drawn with 50% probability. Hydrogen atoms are omitted for clarity.

of an acid and silica gel was necessary for the isomerization. It is interesting to note that other adsorbents such as alumina (acidic, neutral, or basic) and molecular sieves were not effective. This room-temperature isomerization is quite remarkable, as all isomerizations described before were carried out at higher temperature with the exception of photochemical isomerizations. The role of the acid is probably to protonate the N atom of one of the isoquinoline ligands, which leaves a coordination vacancy for the migration of one of the Ir−C bonds to induce the isomerization process. Additional work is required to elucidate the mechanism of this reaction including the unique role played by silica gel.

However, none of the above methods worked as cleanly for isomerizing *mer*-Ir(piq)(ppy)$_2$. Instead, *fac*-Ir(piq)-(ppy)$_2$ was separated in small quantity from a mixture of *fac* compounds obtained in a conventional reaction method[56] by successive chromatography and crystallization steps.

X-ray Structure Determination. The crystal data and structure refinement for *fac*-Ir(piq)$_2$(ppy) are listed in Table 1. An ORTEP diagram is shown in Figure 1. Selected bond angles and distances are listed in Table 2. These structural values, particularly the bond lengths, are within the range typical for other *fac* isomers of tris-C^N cyclometalated Ir(III) complexes reported in the literature. In the previously reported[44] structure determination of *mer*-Ir(piq)$_2$(ppy), the Ir(1)−C(41) bond of the equatorial ppy ligand was found to be about 0.1 Å longer than the Ir(1)−C(16) bond length reported here for the *fac* isomer, clear evidence of a strong *trans* effect of the opposite Ir−C bond. Similar bond lengths have been reported for other *mer* tris-C^N cyclometalated Ir(III) complexes.[52,53]

Electrochemical Properties. The oxidation and reduction potentials of the series *fac*- and *mer*-Ir(piq)$_x$(ppy)$_{3-x}$ (x = 0−3) were measured by second harmonic AC voltammetry (SHACV)[49] in 1:1 CH_3CN/toluene with 0.1 M $TBABF_4$ as the supporting electrolyte. SHACV was chosen over the more familiar cyclic voltammetry because the values of the reduction potentials encountered are very negative and overlap with the reduction of the solvent/electrolyte solution. Solvent background currents are suppressed in SHACV allowing for more exact measurement of redox potentials in this case. Using this technique, three reversible reduction potentials were measured for each complex, except *fac*- and *mer*-Ir(piq)$_2$ppy, for which the third reduction was irreversible. The potentials vs SCE are listed in Table 3. The oxidation potentials were practically identical for all four *fac* complexes, indicating that the piq and ppy ligands have equal electron donor properties. The oxidation potentials of the four *mer* complexes are also very close to each other, but about 90 mV lower than those of the *fac* complexes. The first reduction potentials of the piq-containing complexes show a small trend toward less negative values as the number of piq ligand increases within either the *fac* or *mer* series.

Table 2. Selected Bond Lengths (Å) for *fac*-Ir(piq)$_2$(ppy) and *mer*-Ir(piq)$_2$(ppy)

fac-Ir(piq)$_2$(ppy)[a]		*mer*-Ir(piq)$_2$(ppy)[b]	
Ir(1)−C(27)	1.985(10)	Ir(1)−C(30)	2.029(11)
Ir(1)−C(1)	1.996(9)	Ir(1)−C(15)	1.989(11)
Ir(1)−C(16)	2.003(9)	Ir(1)−C(41)	2.105(11)
Ir(1)−N(1)	2.126(7)	Ir(1)−N(1)	2.036(9)
Ir(1)−N(3)	2.123(8)	Ir(1)−N(2)	2.047(9)
Ir(1)−N(2)	2.150(6)	Ir(1)−N(3)	2.118(11)

[a] This work. [b] Ref 31.

Table 3. Electrochemical Data for Iridium Complexes[a]

compound	E_{ox}	$^1E_{red}$	$^2E_{red}$	$^3E_{red}$
fac-Ir(ppy)$_3$	0.768	−2.265	−2.510	−2.770
fac-Ir(piq)$_3$	0.769	−1.802	−1.989	−2.183
fac-Ir(piq)$_2$(ppy)	0.768	−1.829	−2.021	−2.6[b]
fac-Ir(piq)(ppy)$_2$	0.768	−1.848	−2.328	−2.564
mer-Ir(ppy)$_3$	0.678	−2.230	−2.486	−2.788
mer-Ir(piq)$_3$	0.672	−1.790	−1.983	−2.200
mer-Ir(piq)$_2$(ppy)	0.678	−1.804	−2.052	−2.6[b]
mer-Ir(piq)(ppy)$_2$	0.680	−1.832	−2.333	−2.595

[a] Error ±3 mV. Potentials versus NaCl-saturated SCE. Data obtained in 1:1 CH_3CN/toluene containing 0.1 M $TBABF_4$. The oxidation potential of the reference compound ferrocene measured 0.468 V in this electrolyte. [b] Peak potential for an irreversible, multielectron wave.

Photophysical Properties of *fac*-Ir(piq)$_x$(ppy)$_{3-x}$ (x = 1−3). The absorption spectra in the visible region of the series *fac*-Ir(piq)$_x$(ppy)$_{3-x}$ in 2-MeTHF solution at 295 K are shown in Figure 2. Absorption spectra extending further into the UV are shown in Figure SI-2 in the Supporting Information. By comparison to literature spectra of *fac*-Ir(ppy)$_3$, the absorption at wavelengths longer than 400 nm in the present complexes is mainly associated with the piq ligands. The absorption profile of all three compounds in this region appears very similar, except the molar extinction increases with the number of piq ligands. There appear to be at least four overlapping bands, and these are likely MLCT or ligand-based $\pi-\pi^*$ with strong admixture of MLCT character. While it is not possible to precisely delineate singlet and triplet absorptions, the lowest energy portion of the spectra having relatively low extinction beyond about 580 nm is likely to be substantially triplet in character.

The emission spectra are compared on a normalized basis in Figure 3. The heteroleptic complexes show slight

(56) DeRosa, M. C.; Hodgson, D. J.; Enright, G. D.; Dawson, B.; Evans, C. E. B.; Crutchley, R. J. *J. Am. Chem. Soc.* **2004**, *126*, 7619.

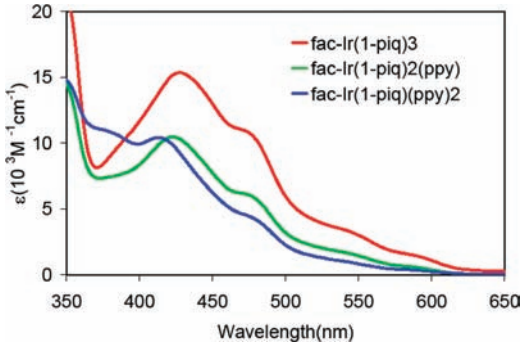

Figure 2. Absorption spectra of the series *fac*-Ir(piq)$_x$(ppy)$_{3-x}$ (x = 1−3) in 2-MeTHF.

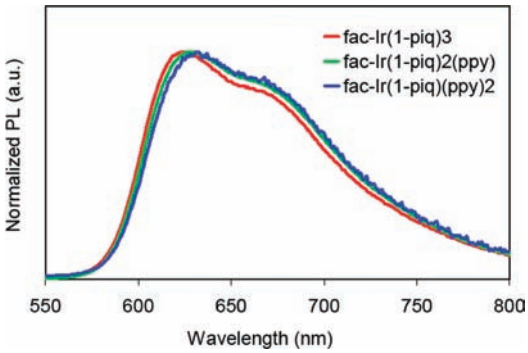

Figure 3. Emission spectra of the series *fac*-Ir(piq)$_x$(ppy)$_{3-x}$ (x = 1−3) in 2-MeTHF at 295 K. Excitation with 458 nm lines of cw Ar ion laser.

Table 4. Emission Maxima, Quantum Yields, and Decay Times of the Series *fac*-Ir(piq)$_x$(ppy)$_{3-x}$ (x = 1−3) in 2-MeTHF at 293 K

compound	λ_{max} (nm)	Φ^a	τ_{obs} (μs)^b
fac-Ir(piq)$_3$	624	0.45	1.25
fac-Ir(piq)$_2$(ppy)	627	0.37	1.39
fac-Ir(piq)(ppy)$_2$	631	0.40	1.38

[a] Error ±10%. [b] Error ±5%.

red shifts relative to the homoleptic, but all three have practically the same band shape and bandwidth. The quantum yields and luminescence decay times in solution are listed in Table 4. In the present study, the solution quantum yield was found to be higher and the decay time longer than in a previous report of *fac*-Ir(piq)$_3$,[5] albeit in a different solvent. The results in Table 4 suggest that quantum yields in solution may be lower for the heteroleptic complexes compared to the homoleptic, but all are still within experimental error of ±10%. The observed decay time for the homoleptic complex in solution is different from the two heteroleptics just at the margin of the estimated experimental error of ±5%.

Samples of the three *fac* compounds doped into PMMA were each prepared by two methods. The first set were castings of ~1 mm thickness and 0.015% concentration by weight prepared by a slow (>2 weeks) evaporation of solvent. The second set was prepared at a higher concentration of 1% by blade coating a thickness of 100 μm of a dichloromethane solution containing the compound and PMMA onto a poly(ethylene terephthalate) (PET) film base. A background fluorescence for the PET support had to be subtracted in the case of the latter set, but consistent emission spectra and decays were obtained with both

Table 5. Quantum Yields at 295 K and Emission Maxima at Selected Temperatures of the Series *fac*-Ir(piq)$_x$(ppy)$_{3-x}$ in PMMA

	Φ^a	λ_{max} (nm)		
compound/temperature	295 K	295 K	90 K	2 K
fac-Ir(piq)$_3$	0.45	616	612	624
fac-Ir(piq)$_2$(ppy)	0.43	617	610	628
fac-Ir(piq)(ppy)$_2$	0.43	614	610	626

[a] Error ±10%.

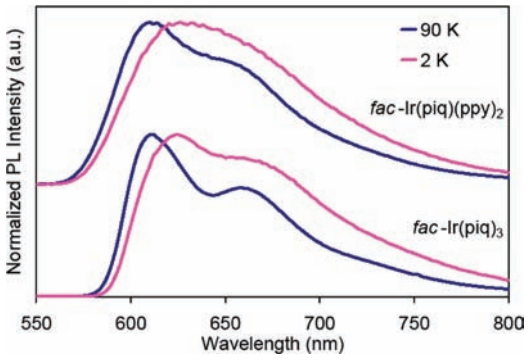

Figure 4. Emission spectra at 90 and 2 K for *fac*-Ir(piq)(ppy)$_2$ and for *fac*-Ir(piq)$_3$ in PMMA host.

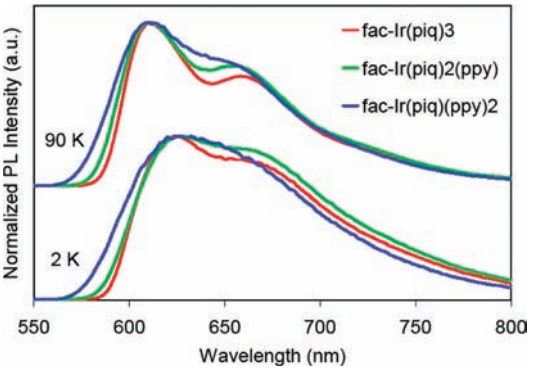

Figure 5. Emission spectra of *fac*-Ir(piq)$_x$(ppy)$_{3-x}$ (x = 1−3) in PMMA host at 90 K and at 2 K.

sets of samples for each respective compound. Only the thick PMMA castings were used for quantum yield determination by an integrating sphere method.

All three *fac* compounds in PMMA at 295 K gave similar quantum yields but blue shifts relative to their 2-MeTHF solutions (cf. Tables 4 and 5). All three of the *fac* compounds showed only a modest sharpening of the emission band and less than 10% change in integrated intensity upon cooling from 295 to 90 K. However, a substantial red shift and change in band shape accompanied by about a 60% intensity decrease was found upon cooling to 2 K. Spectra are compared on a normalized basis at 90 and 2 K in Figure 4 for *fac*-Ir(piq)$_3$ and *fac*-Ir(piq)(ppy)$_2$, while spectra for all three compounds are compared to each other at 90 K and at 2 K in Figure 5. The band shift and shape changes with temperature seen in Figure 5 for the respective compounds are very similar to those previously reported for *fac*-Ir(ppy)$_3$ and may be explained analogously by a well established model.[20] According to that model, the emission at higher temperature is dominated by decays from the second and third sublevels (II and III) of the triplet state, whereas thermalized

emission at sufficiently low temperature originates almost exclusively from the lowest triplet sublevel (I). Emission from II and III acquires intensity by spin−orbit coupling, and thus each comprises a (0,0) transition plus a Franck−Condon vibronic sideband involving the vibrational modes of the molecule. Emission from I is more strongly spin-forbidden, requiring a spin-vibronic interaction to gain intensity, and thus lacking (0,0) intensity but exhibiting (0,1) intensity by Herzberg−Teller coupling to vibrational modes. Individual (0,0) and (0,1) bands are not resolved in amorphous hosts due to inhomogeneous broadening.

As seen in Figure 5, at a given temperature the emission energy is red-shifted and the band shape less broad as the number of piq ligands increases through the series. The spectral changes between $x = 1$ and $x = 2$ are much greater than between $x = 2$ and $x = 3$ piq ligands. While the emission origin energies cannot be accurately determined without detailed analysis of the excitation profiles, rough estimates may be made by considering the energies at which intensity is 25% of the peak maximum intensity. In this manner, the energy shift from $x = 1$ to $x = 3$ was estimated to be 321 and 338 cm^{-1}, respectively, from the two sets of samples. By comparison, the stabilization of the MLCT excited state of $Ru(bpy)_3^{2+}$ due to delocalization over the ligands has been roughly predicted to be about 1000 cm^{-1}.[34]

Emission decays were obtained from 295 K down to 2 K by exciting the samples at 485 nm. For *fac*-Ir(piq)$_3$, four independent experimental runs were conducted including both the thick (0.015%) and the thin (1%) doped PMMA samples. Good reproducibility was obtained, except for one datum at 7 K and one at 14 K that could be discarded as outliers compared to the remaining three data points at the respective temperatures. For *fac*-Ir(piq)$_2$(ppy), one data set each was collected for the thick and the thin PMMA samples and good agreement was obtained. In the case of *fac*-Ir(piq)(ppy)$_2$, only one experimental run using the thick PMMA casting is reported, but three decays were recorded at each temperature, except for room temperature. Good reproducibility among the three replicates at each temperature demonstrated that the sample had thermally equilibrated. Representative logarithmic decay plots for *fac*-Ir(piq)(ppy)$_2$ are shown in Figure SI-3 in Supporting Information. At the lowest temperatures (2 and 7 K), immediately after excitation, there were brief fast decays. This behavior has been observed for $Ru(bpy)_3^{2+}$, and it was concluded that it was due to local heating of the sample by the laser,[57] although there could also be an effect due to slow spin−lattice relaxation.[58,59] Therefore, only the decay after this initial nonthermalized portion was used to fit the observed decay rate, $k_{obs} = 1/\tau_{obs}$, in the cases of the lowest temperature measurements. Otherwise, the decays were nearly single exponential, with some deviation at long times. Deviation from single exponential decay has been observed for other Ir complexes in amorphous hosts and has been interpreted as a variation in photophysical properties due to inhomogeneites in the environment.[28] Here the slope of the initial straight line portion of each logarithmic decay plot was taken as an average k_{obs} for most molecules in the inhomogeneously broadened sample. In the case of *fac*-Ir(piq)(ppy)$_2$, decays were also evaluated by an effective rate constant, $k_{e^2} = 2/t_{e^2}$, where t_{e^2} is time at which the intensity has decreased from its initial value, I_0, to I_0/e^2. (In the case of lowest temperature measurements, the initial intensity was extrapolated from the decay curve after the initial nonthermalized portion). Very similar values of τ_{obs} for *fac*-Ir(piq)(ppy)$_2$ at the respective temperatures (mostly within 5%) were obtained with both methods because there was relatively small deviation from single exponential behavior over this time period.

The observed decay rate of a thermalized triplet excited state may be described as a Boltzmann average by the well-known eq 1:[20,60]

$$k_{obs} = \frac{k_I + k_{II}\exp(-\Delta E_{II}/kT) + k_{III}\exp(-\Delta E_{III}/kT)}{1 + \exp(-\Delta E_{II}/kT) + \exp(-\Delta E_{III}/kT)} \quad (1)$$

The decay rates of the individual sublevels of the triplet state are k_I, k_{II}, and k_{III}, respectively, while k is the Boltzmann constant. ΔE_{II} and ΔE_{III} are the zero-field splitting (ZFS) energies of the second and third triplet sublevels, respectively, above the energy of the lowest triplet sublevel. Each decay rate in eq 1 is the sum of the respective radiative and nonradiative decay rates (e.g., $k_{I,r}$ and $k_{I,nr}$, respectively). Equation 1 holds as long as the decay rate for each sublevel remains constant with temperature.

The experimental k_{obs} data from the initial slope method were fit to eq 1 and the results are listed in Table 6. The temperature dependences of the k_{obs} values for *fac*-Ir(piq)$_3$ and *fac*-Ir(piq)(ppy)$_2$, including replicates, are shown in Figure 6 along with the calculated curves using eq 1 with the parameters obtained from the fits. The data for *fac*-Ir(piq)$_2$(ppy) were very similar to those for *fac*-Ir(piq)$_3$ and were omitted from the figure for clarity. When fit to eq 1, the k_{obs} values evaluated as k_{e^2} for *fac*-Ir(piq)(ppy)$_2$ gave practically the same ZFS and decay rates of the individual sublevels as did the k_{obs} values evaluated by the initial slope method.

As mentioned in the Experimental Section, the *fac*-Ir(piq)(ppy)$_2$ sample contained a persistent impurity of *fac*-Ir(piq)$_2$(ppy). Details of corrections to the photophysical properties of *fac*-Ir(piq)(ppy)$_2$ to account for this impurity are given in the Supporting Information. The concentration of the impurity, 5%, was too small to affect the spectra or quantum yields significantly. The calculated effects of the impurity on the zero-field splittings and decay rates of the triplet sublevels are given in the footnote to Table 6. The differences between the corrected and uncorrected values for these parameters are not significantly larger than the experimental errors.

The results listed in Table 6 show a substantially larger ZFS for *fac*-Ir(piq)(ppy)$_2$ ($\Delta E_{III} = 101$ cm^{-1}) than for fac-Ir(piq)$_3$ (64 cm^{-1}). The value for *fac*-Ir(piq)$_2$(ppy) was

(57) Krausz, E.; Moran, G. *J. Lumin.* **1988**, *42*, 21–27.
(58) Strasser, J.; Homeier, H. H. H.; Yersin, H. *Chem. Phys.* **2000**, *255*, 310–316.
(59) Yersin, H.; Strasser, J. *Coord. Chem. Rev.* **2000**, *208*, 331–364.
(60) Harrigan, R. W.; Crosby, G. A. *J. Chem. Phys.* **1973**, *59*, 3468.

Table 6. Zero-Field Splittings and Decay Rate Constants for Triplet Sublevels Obtained by Fitting eq *1* to Observed Decay Rates of *fac*-Ir(piq)$_x$(ppy)$_{3-x}$ (x = 1−3) in PMMA

compound	ΔE_{II} (σ) (cm^{-1})	ΔE_{III} (σ) (cm^{-1})	k_I (σ) (10^4 s^{-1})	k_{II} (σ) (10^5 s^{-1})	k_{III} (σ) (10^6 s^{-1})
fac-Ir(piq)$_3$	10.5(0.8)	64.4(2.5)	1.76(0.05)	1.90(0.17)	2.37(0.06)
fac-Ir(piq)$_2$(ppy)	9.1(1.1)	65.3(3.4)	1.67(0.08)	1.57(0.19)	2.28(0.08)
fac-Ir(piq)(ppy)$_2$[a]	14.5(1.9)	100.6(5.9)	1.58(0.08)	1.14(0.16)	2.62(0.17)

[a] Values uncorrected for *fac*-Ir(piq)$_2$(ppy) impurity. Corrected values: ΔE_{II} = 15.6(3.1) cm^{-1}, ΔE_{III} = 106.6(7.4) cm^{-1}, k_I = 1.56(0.07) × 10^4 s^{-1}, k_{II} = 0.95(0.21) × 10^5 s^{-1}, k_{III} = 2.78(0.20) × 10^6 s^{-1}.

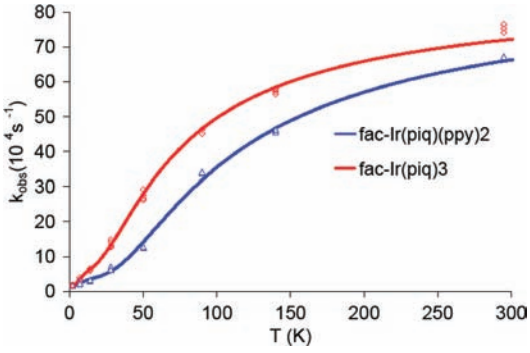

Figure 6. Temperature dependence of observed decay rates for *fac*-Ir(piq)(ppy)$_2$ and *fac*-Ir(piq)$_3$ in PMMA. Open symbols: experimental data points. Solid curves: Calculated according to fit of eq 1 with parameters listed in Table 6.

within experimental error of that for *fac*-Ir(piq)$_3$. From analysis of deviation from single exponential decay of Ir complexes in another report, it has been found that values of the ZFS of a single compound can vary over a similar range due to inhomogeneous broadening in a sample.[28] However, in the present study ZFS from fits to decays of similar compounds were evaluated in a uniform manner. Therefore, the larger ZFS for *fac*-Ir(piq)(ppy)$_2$ was concluded to be a molecular property and not an effect of inhomogeneous broadening.

In studies of several analogous series of homo- and heteroleptic tris(diimine)Ru(II) complexes in single crystal hosts, the ZFS was found in all cases to be smaller for the homoleptic compounds by a similar percentage as was observed in the present study.[40,42] This finding was interpreted as evidence that the excited state has less MLCT character in the homoleptic case as a result of delocalization over three ligands compared to a localized case when only one emissive ligand was present.[40] On the other hand, it was also pointed out that the increasing ZFS correlated with increasing emission energy in at least one of those studies, complicating the interpretation.[42] The present series of complexes has the advantage that the matched oxidation potentials through the series suggest that there should be minimal energy shifts due to differences in electron donor effects of the piq and ppy ligand(s). Therefore, the interpretation would be applicable that the smaller ZFS observed in *fac*-Ir(piq)$_3$ and *fac*-Ir(piq)$_2$(ppy) relative to that in *fac*-Ir(piq)(ppy)$_2$ indicates delocalization in the first two complexes. While the two piq ligands in *fac*-Ir(piq)$_2$(ppy) are not equivalent, they could be accidentally degenerate or nearly so. There does not seem to be a large effect on ZFS of increasing delocalization from two piq ligands to three.

In contrast, the decay rates for the individual sublevels of the triplet state in the three *fac* compounds do not differ by nearly as much as the ZFS do, except in the case of k_{II} for *fac*-Ir(piq)(ppy)$_2$ that is significantly *lower* than the values obtained for the other two compounds. Both the ZFS and the decay rates arise from spin−orbit coupling interactions and depend upon degree of metal orbital character in the states involved in the emission. The decay rate depends on coupling to singlet excited state(s) and the oscillator strength of the optical transition from that singlet excited state to the ground state, while ZFS is thought to depend more dominantly on spin−orbit coupling to the next higher lying ^{3}MLCT.[28] Thus the large difference in ZFS but generally smaller difference in decay rates among the present compounds was unexpected, but not necessarily contradictory.

Electroluminescence with *fac*-Ir(piq)$_x$(ppy)$_{3-x}$ (x = 1−3). The three *fac* compounds were also evaluated in vapor-deposited OLEDs having the following order of layers: ITO (250 Å) | CFx | NPB (750 Å) | BAlq-13 + 15% NPB + 4% *fac*-Ir(piq)$_x$(ppy)$_{3-x}$ (350 Å) | BAlq-13 (100 Å) | Alq (400 Å) | LiF (5 Å) | Al (1200 Å), where CFx is a coating produced by plasma-assisted polymerization of CHF_3,[61] NPB is the hole-transporting material 4,4′-bis[*N*-(1-naphthyl)-*N*-phenylamino]biphenyl, BAlq-13 is bis(2-methyl-quinolin-8-olato)(2,6-diphenylphenolato)aluminum(III),[50] and Alq is the electron-transporting material *mer*-tris(quinolin-8-olato)aluminum(III). This device formulation was previously reported with *fac*-Ir(piq)$_3$ as dopant,[50] except that the blue aluminum chelate cohost was a close analogue of the one employed here, BAlq-13. Detailed characterization of that device formulation, including dopant concentration and current density dependencies, was reported previously.[50] Here we compare electroluminescence (EL) performance of the three *fac* compounds in Table 7 at the current density (5 mA/cm^2) that gave the maximum EQE for each. The EL spectra of the three compounds are shown on a normalized basis in Figure 7. As was observed with photoluminescence spectra in PMMA host, the EL spectra show a decrease in bandwidth and a red shift of the emission as the number of piq ligands in the complex increases. In this host material, the red shift from x = 1 to x = 3 is roughly 176 cm^{-1} as judged by the points at which the EL intensity on the high energy side is at 25% of the peak maximum intensity. Although the quantum yield in PMMA was measured to be nearly the same for all three *fac* compounds (0.43−0.45) within the experimental error (±10%), the electroluminescence efficiency, albeit using different host materials in the OLEDs, suggests that the QY likely is less for x = 1 than x = 3. The lower quantum efficiency would be at least consistent with an increased nonradiative decay rate due to the increased excited state distortion in x = 1 relative to x = 3 as evidenced by the broadened band shape.

(61) Hung, L. S.; Zheng, L. R.; Mason, M. G. *Appl. Phys. Lett.* **2001**, *78*, 673–676.

Table 7. EL Performance of the Devices ITO (250 Å) | CFx | NPB (750 Å) | BAlq-13 + 15% NPB + 4% *fac*-Ir(piq)$_x$(ppy)$_{3-x}$ (350 Å) | BAlq-13 (100 Å) | Alq (400 Å) | LiF (5 Å) | Al (1200 Å) for $x = 1-3$ at 5 mA/cm^2

compound	voltage	yield (cd/A)	EQE (% ph/e)	λ_{max} (nm)	fwhm (nm)	CIE X,Y
fac-Ir(piq)$_3$	7.19	11.4	12.5	622	83.5	0.664, 0.331
fac-Ir(piq)$_2$(ppy)	6.91	10.5	11.4	621	89.0	0.659, 0.335
fac-Ir(piq) (ppy)$_2$	6.96	10.5	10.8	619	94.3	0.651, 0.342

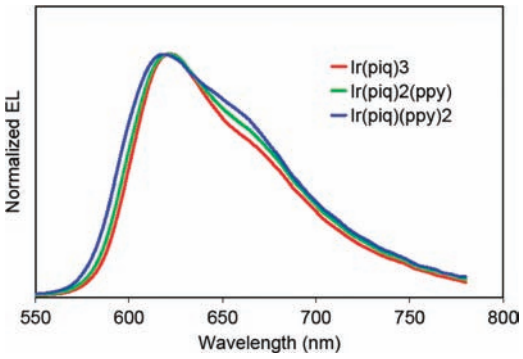

Figure 7. Normalized EL spectra of the devices ITO (250 Å) | CFx | NPB (750 Å) | BAlq-13 + 15% NPB + 4% *fac*-Ir(piq)$_x$(ppy)$_{3-x}$ (350 Å) | BAlq-13 (100 Å) | Alq (400 Å) | LiF (5 Å) | Al (1200 Å) for $x = 1-3$ at 5 mA/cm^2.

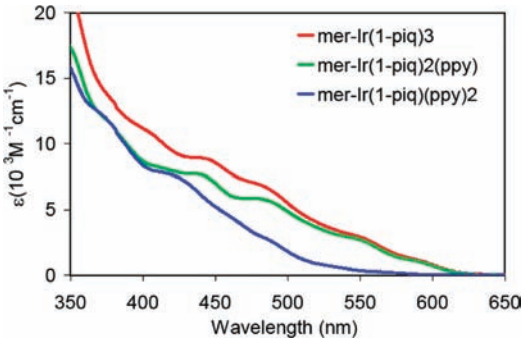

Figure 8. Absorption spectra of the series *mer*-Ir(piq)$_x$(ppy)$_{3-x}$ in 2-MeTHF at 295 K.

According to classical ray optics, the optical outcoupling is about 22% for bottom-emitting devices such as these.[17] With this estimate and the photoluminescence quantum yields of the dopants, it appears from the EQE values recorded here that the excitons formed by electron−hole recombination in this device structure were very effectively trapped by the phosphorescent iridium dopants.

It should be mentioned that the vapor deposition temperature for *fac*-Ir(piq)$_2$(ppy) in OLED device fabrication is lower by about 35 °C than that for *fac*-Ir(piq)$_3$ at the same deposition rate, which could be an advantage for the heteroleptic compound since it has shown comparable EQE of OLED devices. Subsequent vapor pressure measurement revealed that the greater volatility of *fac*-Ir(piq)$_2$(ppy) relative to that of *fac*-Ir(piq)$_3$ arises from an increased entropy of sublimation, not from any significant difference in enthalpy of sublimation (see Supporting Information).

Photophysical Properties of *mer*-Ir(piq)$_x$(ppy)$_{3-x}$ ($x = 1-3$). The absorption spectra in the visible region for the three *mer* complexes in 2-MeTHF solution at 295 K are shown in Figure 8. Absorption spectra extending further into the UV are shown in Figure SI-4 in the Supporting Information. The absorption spectra appear to contain at least five poorly resolved bands of steadily increasing extinction with increasing energy, similar in appearance to spectra of other reported *mer* cyclometalated complexes of Ir(III).[53] The *mer*-Ir(piq)(ppy)$_2$ shows a substantial blue shift on the order of 30 nm relative to the other two *mer* complexes, which have quite similar features to each other. The low energy region of the absorption for *fac*- and *mer*-Ir(piq)(ppy)$_2$ is shown on an expanded scale in Figure SI-5, Supporting Information. While the lowest energy absorption bands are not clearly resolved, this *mer* complex appears to be blue-shifted by about 25−35 nm relative to the *fac* complex in solution. The extinction of the *mer*-Ir(piq)(ppy)$_2$ is about 190 M^{-1} cm^{-1} at 570 nm, while the *fac*-Ir(piq)(ppy)$_2$ complex has an extinction of about 280 M^{-1} cm^{-1} at 595 nm.

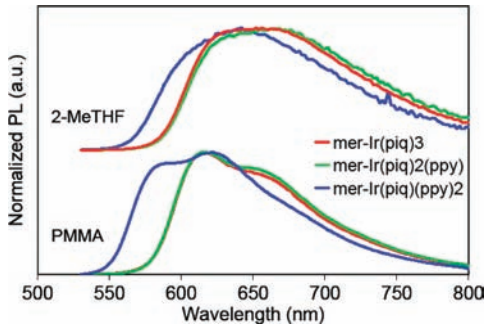

Figure 9. Emission spectra for the series *mer*-Ir(piq)$_x$(ppy)$_{3-x}$ ($x = 1-3$) in 2-MeTHF (top) and PMMA host (bottom) at 293 K. Excitation source was the 458 nm line of an Ar ion laser.

The emission spectra in 2-MeTHF solution of the three *mer* complexes (Figure 9, top) show the blue shift of about 30 nm very distinctly for the *mer*-Ir(piq)(ppy)$_2$ relative to the other two *mer* complexes. The *mer* complexes all display the broad band shape, low quantum yield, and short lifetimes (Table 8) relative to the *fac* complexes (Table 4) that are characteristic of other *mer* C^N-cyclometalated complexes in solution.[53]

We were not able to obtain reliable quantum yields for the *mer* isomers in PMMA with the method of preparing thick castings of doped PMMA because this method involves a slow drying of the castings over a 2−3 week period, during which time there was some decomposition of the *mer* complexes. In the case of *mer*-Ir(piq)(ppy)$_2$, a green emission was obtained from the casting that appeared to be from an adduct of the Ir(ppy)$_2$ fragment after loss of the lone piq ligand that had been at the equatorial position in the *mer* complex. On the other hand, the quick-drying thin films used for the spectroscopic and decay measurements did not show evidence for this degradation. These coatings were used for the spectral and luminescence decay measurements of the *mer* complexes in PMMA.

Compared to their emission spectra in solution, the *mer* complexes in PMMA host exhibit less broad bandshapes (Figure 9, bottom). Longer decay times were observed in

Table 8. Emission Maxima, Quantum Yields, and Decay Times of the Series *mer*-Ir(piq)$_x$(ppy)$_{3-x}$ in 2-MeTHF at 293 K

compound	λ_{max} (nm)	Φ	τ_{obs} (μs)
mer-Ir(piq)$_3$	656	0.072	0.22
mer-Ir(piq)$_2$(ppy)	654	0.066	0.20
mer-Ir(piq)(ppy)$_2$	642	0.094	0.44

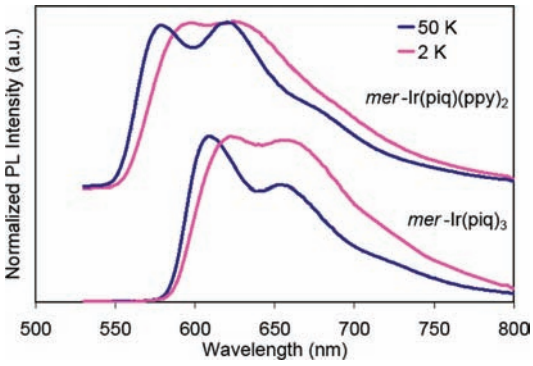

Figure 10. Emission spectra at 50 and 2 K of *mer*-Ir(piq)(ppy)$_2$ (top) and *mer*-Ir(piq)$_3$ (bottom) at 1% by weight in PMMA.

PMMA host at room temperature (vide infra) suggesting that the quantum yields are also much higher in the doped solid film. If so, the broad bandshapes and low quantum yields of the *mer* isomers seem to be characteristic behaviors in solution that do not occur in the doped solid films. We speculate that the behavior in solution is related to the weaker bonding of the ligand in the equatorial position, as indicated for example by the relatively long bond lengths of the ppy ligand in the case of *mer*-Ir(piq)$_2$(ppy)[44] and also by structure determinations of other *mer* complexes.[52,53]

Like the *fac* complexes, each of the *mer* complexes showed red shifts and band shape changes in PMMA at the lowest temperatures, as illustrated for *mer*-Ir(piq)(ppy)$_2$ and *mer*-Ir(piq)$_3$ in Figure 10. The λ_{max} values for each complex in PMMA at selected temperatures are listed in Table 9. The integrated intensity of each *mer* complex emission followed a similar temperature dependence as for the *fac* compounds. In the previous communication,[44] it was shown that the *mer*-Ir(piq)$_3$ and *mer*-Ir(piq)$_2$(ppy) have nearly the same emission wavelengths and band shape as *fac*-Ir(piq)$_3$ in PMMA host. In contrast, *mer*-Ir(piq)(ppy)$_2$ is blue-shifted from *fac*-Ir(piq)(ppy)$_2$ by some 685 cm^{-1}, as judged from the points at which the emission intensity on the high energy side is 25% of the peak maximum intensity of the spectra at 50 K.

The phosphorescent decays of the *mer* complexes showed a greater deviation from single exponential behavior than the *fac* compounds. Several representative decays are shown in Figure SI-6 of the Supporting Information. This was especially the situation at room temperature and again at low temperatures. We found the method of taking the slope of an initial portion of the logarithmic decay plot to be highly subjective and therefore unreliable. In order to make consistent estimates of average decay, we found it best to evaluate the effective observed decay rate constants, k_{e^2}, as described in the preceding section. The decay rates evaluated in this manner were fit to eq 1, and the results are listed in Table 10. The experimental k_{e^2} and calculated curves according to eq 1

Table 9. Emission Maxima of the Series *mer*-Ir(piq)$_x$(ppy)$_{3-x}$ in PMMA at Selected Temperatures

	λ_{max} (nm)		
compound/ temperature	293 K	50 K	2 K
mer-Ir(piq)$_3$	616	608	622
mer-Ir(piq)$_2$(ppy)	616	610	622
mer-Ir(piq)(ppy)$_2$	590[a]	578[a]	598[a]

[a] First emission maximum selected for table entry even though vibronic sideband was equal or greater in intensity.

are shown in Figure 11. Because of the extent of nonexponential behavior and lack of replicate data points, these results must be regarded as preliminary, as reflected in the higher uncertainties listed in Table 10. The ZFS could not be distinguished among the three *mer* compounds as a consequence of the large uncertainties. However, it may be concluded that the ZFS of *mer*-Ir(piq)(ppy)$_2$ is smaller and the decay rate in the high temperature limit, dominated by k_{III}, is clearly slower than that of *fac*-Ir(piq)(ppy)$_2$.

In view of the large amount of evidence that the excited states of related compounds are localized in solution, it is not plausible that the blue shift of *mer*-Ir(piq)(ppy)$_2$ relative to the other two *mer* compounds observed in solution as well as in PMMA host could be explained as a difference caused by a localized vs delocalized excited states. Moreover, the blue shift, smaller ZFS, and slower decay rate of *mer*-Ir(piq)(ppy)$_2$ relative to that of *fac*-Ir(piq)(ppy)$_2$ must be due to differences in the geometrical environment of the piq ligand in the two complexes. The crystal structures of *mer*-Ir(piq)(ppy)$_2$ and *fac*-Ir(piq)(ppy)$_2$ are not available. But by analogy to the structures of *mer*-Ir(piq)$_2$(ppy) and *fac*-Ir(piq)$_2$(ppy), it may be expected that the Ir−C bond length to the piq ligand in *mer*-Ir(piq)(ppy)$_2$ is lengthened by about 0.1 Å relative to that in *fac*-Ir(piq)(ppy)$_2$. It may be expected that such a significant bond lengthening would result in less overlap between the Ir and piq ligand. Decreased MLCT character in the excited state readily explains the differences in photophysical properties between *fac*- and *mer*-Ir(piq)(ppy)$_2$.

In view of the higher energy excited state associated with the ligand in the equatorial position of the cyclometalated *mer* complexes, it is reasonable to expect that the photophysical properties of *mer*-Ir(piq)$_3$ and *mer*-Ir(piq)$_2$(ppy) should be the same. From the data in Figure 11, this appears to be the case. But it is not possible to make a detailed comparison of these compounds to the *fac* analogues due to the large uncertainty in the fits of the decay data.

Conclusions

The photophysical properties of *fac*-Ir(piq)$_x$(ppy)$_{3-x}$ (x = 1−3) in 2-MeTHF solution were all very similar, giving no reason to doubt that the thermalized excited states are localized onto single piq ligands in solution. However, in PMMA host, the emissive states in *fac*-Ir(piq)$_3$ and *fac*-Ir(piq)$_2$(ppy) show smaller ZFS, a red shift, and a less broad band shape relative to those of *fac*-Ir(piq)(ppy)$_2$ in which the excited state must be localized on the lone piq ligand. In contrast, the decay rates of the *fac* compounds do not show differences in proportion to the differences in ZFS. On

Table 10. Zero-Field Splittings and Decay Rate Constants of Triplet Sublevels for the Series *mer*-Ir(piq)$_x$(ppy)$_{3-x}$ (x = 1−3) in PMMA Obtained by Fitting eq *1* to Observed Decay Rates that Were Evaluated As the Effective Decay Rates, k_{e2}, Described in Text

compound	ΔE_{II} (σ) (cm^{-1})	ΔE_{III} (σ) (cm^{-1})	k_I (σ) (10^4 s^{-1})	k_{II} (σ) (10^5 s^{-1})	k_{III} (σ) (10^6 s^{-1})
mer-Ir(piq)$_3$	13.0(3.2)	68.2(8.8)	2.39(0.22)	2.09(0.67)	2.51(0.22)
mer-Ir(piq)$_2$(ppy)	12.8(3.5)	77.3(13.0)	2.14(0.27)	2.19(0.76)	2.69(0.33)
mer-Ir(piq)(ppy)$_2$	11.9(1.6)	59.6(11.6)	1.58(0.11)	2.81(0.58)	1.22(0.01)

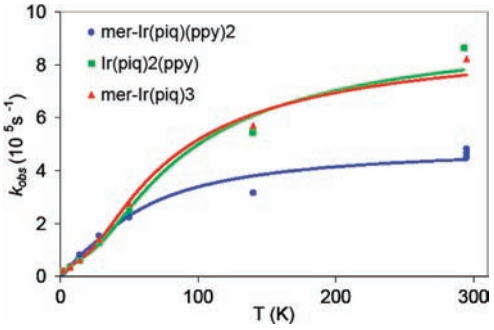

Figure 11. Temperature dependence of observed decay rates for the series *mer*-Ir(piq)$_x$(ppy)$_{3-x}$ in PMMA at 1 wt %. Observed decay rates evaluated as effective decay rates, k_{e2}, as described in text. Symbols: experimental data points. Curves: calculated according to fit of eq 1 with parameters listed in Table 10.

balance, we favor a conclusion from these observations that the emissive states in *fac*-Ir(piq)$_3$ and *fac*-Ir(piq)$_2$(ppy) are delocalized over the piq ligands and thus contain relatively less MLCT character than *fac*-Ir(piq)(ppy)$_2$ in the PMMA matrix, and by extension probably also in amorphous hosts used for OLEDs. The EQE of the OLEDs is perhaps a more sensitive indicator of photoluminescence quantum yield than the determination of the doped PMMA castings in the integrating sphere. The OLED performance comparison suggests a lower quantum yield for *fac*-Ir(piq)(ppy)$_2$ relative to *fac*-Ir(piq)$_3$, implying a faster nonradiative decay rate, consistent with a larger excited state distortion as evidenced by the broader band shape.

The low quantum yield and broad band shape that are generally regarded as characteristics of the cyclometalated *mer* Ir(III) complexes appear to be their properties in solution because the bandshapes were sharper and decay rates were slower in PMMA host. The blue shift, slower decay rates, and smaller ZFS exhibited by *mer*-Ir(piq)(ppy)$_2$ relative to *fac*-Ir(piq)(ppy)$_2$ in PMMA host may be interpreted as evidence that the excited state in the former has relatively less MLCT character and more $\pi-\pi^*$ character. This conclusion may also be inferred from X-ray structure determinations that show a relative lengthening of the Ir−C bond of the ligand in *mer* complexes that is *trans* to the Ir−C bonds of the other two ligands. The photophysical properties of *mer*-Ir(piq)$_3$ and *mer*-Ir(piq)$_2$(ppy) in PMMA appear to be similar to each other, but decay rates and ZFS could not be accurately compared to those of the *fac* analogues because of larger deviations from single-exponential decay exhibited by the *mer* complexes.

Acknowledgment. We thank Dr. Christopher Brown and Mr. Vincent Bakos for supply of some materials used in this study; Dr. Michael Landry and Mrs. Debra Blondell for measurement of vapor pressures; Mr. Joseph Hodes, Mr. Robert Schultz, Mr. Thomas Marchincin, and Dr. Steven Switalski for assistance with the photophysical measurements; Mr. Dustin Comfort for producing the OLEDs and maintaining the coating machine; Prof. James McCusker, Michigan state University, for helpful discussions.

Supporting Information Available: Crystallographic data in CIF format for *fac*-Ir(piq)$_2$(ppy), solid state isomerization of *mer*-Ir(piq)$_2$(ppy), vapor pressure measurements, additional photophysical data, corrections on the photophysical data obtained for the sample of *fac*-Ir(piq)(ppy)$_2$, and proton NMR spectra of all three facial compounds. This material is available free of charge via the Internet at http://pubs.acs.org.